

# Forecasting Seasonal Influenza Epidemics with Physics-Informed Neural Networks

Martina Rama<sup>1,2</sup>, Gabriele Santin<sup>3</sup>, Giulia Cencetti<sup>4</sup>, Michele Tizzoni<sup>5</sup>, and Bruno Lepri<sup>2</sup>

<sup>1</sup>Department of Information Engineering and Computer Science, University of Trento, Trento (Italy)

<sup>2</sup>Mobile and Social Computing (MobS) Lab, Fondazione Bruno Kessler (FBK), Trento (Italy)

<sup>3</sup>Department of Environmental Sciences, Informatics and Statistics, University of Venice, Venice (Italy)

<sup>4</sup>Centre de Physique Théorique, CNRS, Marseille (France)

<sup>5</sup>Department of Sociology and Social Research, University of Trento, Trento (Italy)

June 5, 2025

## Abstract

Accurate epidemic forecasting is critical for informing public health decisions and timely interventions. While Physics-Informed Neural Networks (PINNs) have shown promise in various scientific domains, their application to real-time epidemic forecasting remains limited. The reasons are mainly due to the intrinsic difficulty of the task and the tendency to fully leveraging their learning and inference potential, which, however, often results in non-optimal forecasting frameworks. Here, we present SIR-INN, a hybrid forecasting framework that integrates the mechanistic structure of the classical Susceptible-Infectious-Recovered (SIR) model into a neural network architecture. Trained once on synthetic epidemic scenarios, the model is able to generalize across epidemic conditions without retraining. From limited and noisy observations, SIR-INN infers key transmission parameters via Markov chain Monte Carlo (MCMC) generating probabilistic short- and long-term forecasts. We validate SIR-INN using national influenza data from the Italian National Institute of Health, in the 2023-2024 and 2024-2025 seasons. The model performs competitively with current state-of-the-art approaches, particularly in terms of Mean Absolute Error (MAE) and Weighted Interval Score (WIS). It shows accurate predictive performance in nearly all phases of the outbreak, with improved accuracy observed for the 2024–2025 influenza season. Credible uncertainty intervals are consistently maintained, despite occasional shortcomings in

coverage. SIR-INN offers a computationally efficient, interpretable, and generalizable solution for epidemic forecasting, appropriately leveraging the framework’s hybrid design. Its ability to provide real-time predictions of epidemic dynamics, together with uncertainty quantification, makes it a promising tool for real-world epidemic forecasting.

**Keywords:** Physics-informed neural network, Epidemic modeling, Epidemic forecasting, Seasonal influenza

## 1 Introduction

In recent years, numerical modeling for epidemic forecasting has become a key tool for public health. Short-term forecasts of the epidemic burden, such as the expected number of cases, hospitalizations, or deaths, can inform policymaking and provide situational awareness to respond effectively with targeted intervention strategies [Desai et al., 2019, Lauer et al., 2021]. Over the years, different epidemic forecasting approaches have been adopted to predict the temporal dynamics of dengue [Johansson et al., 2019], Ebola [Viboud et al., 2018], seasonal influenza [Biggerstaff et al., 2016, Brownstein et al., 2017], COVID-19 [Sherratt et al., 2023, Wolfram et al., 2023] and many other diseases [Del Valle et al., 2018, Holcomb et al., 2023].

On the one hand, recent developments in the field have highlighted the numerous advantages of using ensemble modeling strategies based on large collaborative efforts [Reich et al., 2019, Fox et al., 2024, Fiandrino et al., 2025]. At the same time, the most effective standalone approaches generally combine statistical or machine learning techniques with conceptual models that incorporate infectious disease transmission dynamics, either explicitly through compartmental models or implicitly through factors such as seasonality or recent trends in observed data [Lopez et al., 2024, Ray et al., 2025]. However, the use of such hybrid models is still limited in real-world applications, as demonstrated by a recent review of COVID-19 modeling studies in the United States, showing that only 13% of the research teams adopted a hybrid methodology for pandemic forecasting [Nixon et al., 2022].

In general, hybrid methods have been developed to preserve the knowledge of the spreading mechanism, derived from mechanistic modelization, while simultaneously leveraging the data-driven learning capabilities and flexibility of machine learning models [Karniadakis et al., 2021, O’Dea and Drake, 2022, Ye et al., 2025]. Among hybrid models, a promising framework is emerging rapidly within the field of epidemiology: the Physics-Informed Neural Network (PINN) [Raissi et al., 2019]. PINNs are capable of incorporating the observed data and mathematical models described by Partial Differential Equations (PDEs) through a regularization mechanism endowed with the neural network. Furthermore, compared with purely data-driven approaches, a PINN can take advantage of few and noisy data, while still ensuring robustness and generalization capabilities for its physically consistent predictions [Raissi et al., 2019, Karniadakis et al., 2021, Cuomo et al., 2022].

For these reasons, PINNs are successfully used for a wide variety of applications such as aerodynamics, fluid mechanics, biology, and epidemiology [Lagergren et al., 2020, Mao et al., 2020, Cai et al., 2021]. Specifically, within the epidemiological context, the integration of prior epidemiological knowledge (derived from mechanistic models) enables the neural network to serve as an efficient surrogate, accurately learning the dynamics of disease spread and inferring disease-related parameters [Shaier et al., 2021, Bertaglia et al., 2022, Ning et al.,

2023a,b].

However, despite the fact that the literature on epidemiological PINNs is becoming wide and ubiquitous, the prediction of real-time epidemic scenarios with PINNs has not been extensively explored. Some recent efforts have begun to address this gap. [Madden et al. \[2024\]](#) have proposed to integrate a time series SIR model (TSIR) with Physics-Informed Neural Networks (PINNs) that improves both forecast and parameter inferences of measles dynamics. [Berkhahn and Ehrhardt \[2022\]](#) implemented a PINN for COVID-19 modelization and future outbreak scenario generation. [Millevoi et al. \[2024\]](#) implemented a multiple PINNs framework investigating joint and split approaches to estimate temporal changes in model parameters and state variables, also providing a short-term forecast application on Italian COVID-19 data. Epidemiologically-Informed Neural Networks (EINNs) framework, introduced by [Rodríguez et al. \[2023\]](#), combines a time module and a feature module to leverage multiple data sources for both short-term and long-term forecasting. Finally, [Kharazmi et al. \[2021\]](#) investigated several epidemiological models adopting the PINNs approach that uses multiple neural networks, identifying time-dependent parameters and forecasting with uncertainty quantification.

Most of these works adopt a framework that simultaneously addresses both forward and inverse problems, fully exploiting the potential of PINNs. Alternatively or jointly, some of the aforementioned approaches rely on an extensive use of different neural networks, employing them independently to solve specific tasks (e.g., learning the compartments of the PDEs model, finding the unknown parameters) and subsequently combining their results. In either case, when aiming for real-time forecasting, a weakness emerges: the designed framework requires neural network retraining whenever new observations (or new epidemic scenarios) become available, thus increasing both the computational cost and the delay in receiving results. This also restricts the generalizability of a single pre-trained neural network. Moreover, by design, the neural network evaluation produces one single deterministic output as forecast trajectories. As a drawback, in almost all of these cases, there is no uncertainty analysis with respect to the forecasting process, which, instead, is provided by statistical inferential approaches and stochastic simulation studies [[Bracher et al., 2021](#), [Sherratt et al., 2023](#)].

To address these limitations while preserving the known benefits and potential of a hybrid approach, we propose here a novel framework for epidemic forecasting, namely Susceptible-Infectious-Recovered (SIR) - Informed Neural Network (SIR-INN). In particular, we construct a single PINN taking advantage of the simplicity and modeling ability in describing different epidemic dynamics of the Susceptible-Infectious-Recovered (SIR) model. The prior epidemiological knowledge embedded in the neural network architecture is directly derived from the differential equations underlying the SIR compartmental model, with constant transition rates. Our PINN is trained once on synthetic observations of epidemic scenarios that are close to the real ones in a temporal-epidemic domain that considers as variables both the epidemic parameters and the time. This enables our model to efficiently learn a wide range of disease dynamics, generalizing its understanding to the transmission patterns of other infectious diseases. Thus, starting from a limited and noisy set of observations, the pre-trained SIR-INN is able to estimate, via the Markov chain Monte Carlo (MCMC) method, the parameters that characterize a Susceptible-Infectious-Recovered (SIR)-based epidemic dynamics. Finally, by exploiting these estimated parameters, our model can efficiently forecast future time windows.

To validate our proposed framework in a real-world epidemic scenario, we use national

data from the Italian seasonal influenza surveillance system, provided by the Italian National Institute of Health (ISS) [[Istituto Superiore di Sanità, 2020](#)]. In particular, we perform forecasting simulations four weeks and ten weeks ahead for both the 2023-2024 and 2024-2025 influenza seasons. Furthermore, we compare our results with state-of-the-art approaches for seasonal influenza forecasting, presented in the Influcast Hub [[InfluCast, 2025](#)], and adopting the same evaluation metrics as done by [Fiandrino et al. \[2025\]](#). Such results and comparisons suggest that our SIR-INN offers an efficient, cost-effective, and accurate hybrid alternative for real-world epidemic forecasting. It maintains high predictive accuracy even in long-term horizons and across multiple epidemic scenarios, while ensuring both generalizability and reliable uncertainty quantification.

The remainder of the paper is structured as follows. In Section 2, we present the structure of SIR-INN methodology, highlighting the three phases of model approximation, parameter inference, and forecasting. The details of the implementation of all components of the methodology are reported in Section 3. The numerical results of the application of the proposed framework in seasonal influenza scenarios are provided in Section 4. Finally, we summarize our work and derive our conclusions in Section 5.

## 2 Methods

The SIR-INN framework presented in this work mainly consists of three consecutive and related steps: the Physics-Informed Neural Network (PINN) training, the inference of the disease features, and, finally, the forecasting of the future disease states.

In the first phase, described in detail in Section 2.1, we implement a SIR-based PINN. Specifically, we insert as a regularization term into the loss function of a neural network, the ordinary differential equations of a SIR epidemic model. Then, we train the PINN on synthetic data close to real disease scenarios. The following steps leverage this pre-trained PINN with the aim of forecasting the disease spreading process starting from a few noisy observations. In particular, Section 2.2 describes how, from a selected time window of observations, we infer via the Markov chain Monte Carlo (MCMC) method the parameters that characterize the disease-spreading dynamics. Then, evaluating our pre-trained PINN model on these estimated parameters and on a future time window, we can do short-term or long-term disease forecasting. This last step is explained in detail in Section 2.3.

### 2.1 SIR model approximation via PINN

Physics-Informed Neural Networks (PINNs) are universal function approximators efficiently endowed with physical knowledge described in terms of systems of Ordinary Differential Equations (ODEs) or Partial Differential Equations (PDEs) [[Raissi et al., 2019](#)].

Here, we focus on a PINN that incorporates an epidemic spreading dynamic as physical knowledge, while fitting some synthetic data close to real epidemic scenarios. In this setting, a well-known and widely used compartmental model is the SIR epidemic model [[Kermack](#)

and McKendrick, 1927], defined by:

$$\begin{cases} \frac{dS(t)}{dt} &= -\frac{\beta}{N}S(t)I(t), \\ \frac{dI(t)}{dt} &= \frac{\beta}{N}S(t)I(t) - \gamma I(t), \\ \frac{dR(t)}{dt} &= \gamma I(t), \end{cases} \quad (1)$$

where  $S : [t_0, T] \rightarrow \mathbb{R}$  represents the total number of susceptibles,  $I : [t_0, T] \rightarrow \mathbb{R}$  the number of infected individuals, and  $R : [t_0, T] \rightarrow \mathbb{R}$  the number of removed individuals. Individuals are transferred between compartments through two transition rates:  $\beta \in \mathbb{R}_{\geq 0}$ , the epidemic contact or transmission rate, and  $\gamma \in \mathbb{R}_{\geq 0}$ , the removal rate (recovered or mortality). A fundamental threshold quantity for the analysis of disease spread is the so-called basic reproduction number  $R_0 = \beta/\gamma$  that represents the expected number of new infections produced by a single infected individual, during their infectious period, when introduced into a population where all subjects are susceptible [Heffernan et al., 2005].

Given the initial conditions  $S(0), I(0), R(0)$ , the system is fully specified, and letting  $N : [t_0, T] \rightarrow \mathbb{R}$  be the total size of the population at time  $t = 0$ , we have  $N(t) = S(0) + I(0) + R(0) > 0$  for all  $t \in [t_0, T]$ , which implies that  $\frac{dN(t)}{dt} = 0$ . Note also that the epidemic dynamics does not allow any effects of births and deaths on the populations since the time scale of epidemic is assumed to be shorter with respect to the vital dynamics mechanism.

The first step, illustrated in Figure 1, is to implement a PINN that learns the epidemic model SIR defined by Equations 1. This ODEs system can be formulated as of a parametrized non-linear ODEs system

$$\frac{du(t; \lambda)}{dt} + F[u(t; \lambda); \lambda] = 0, \quad t \in [t_0, T], \quad (2)$$

where  $\lambda := (\beta, \gamma, N) \in \mathbb{R}_{>0}^3$  are the parameters of System 1,  $F[u; \lambda]$  is the parametric non-linear differential operator; and  $u : [t_0, T] \times \mathbb{R}^3 \rightarrow \mathbb{R}^3$ ,  $u(t; \lambda) := (S(t), I(t), R(t)) \in \mathbb{R}^3$  is the solution map [Folland, 1995, Evans, 2022].

With the framework defined by Equations 2, the objective of the PINN approach is as follows. Given fixed model parameters  $\lambda \in \mathbb{R}^m$ , find a neural network  $u_N^{\omega, b}(t; \lambda)$  that approximates the solution  $u(t; \lambda)$  of the ODEs system. Here,  $\omega$  and  $b$  represent learnable weights and biases on the neural network. To ensure that the neural network that approximates the solution  $u(t; \lambda)$  efficiently learns a variety of epidemic scenarios, we extend the temporal domain of the function approximator to a temporal-epidemic domain that considers as variables the epidemic parameters in addition to the time variable. Hence, we construct the PINN as a function  $u_N^{\omega, b} : \mathcal{T} \times \mathcal{B} \times \Gamma \rightarrow \mathbb{R}^3$ , namely  $u_N(t, \beta, \gamma)$ , with the aim of approximate the solution  $u(t; \beta, \gamma, N)$ . In particular,  $\mathcal{T} = [t_0, t_{max}]$ ,  $\mathcal{B} = [\beta_0, \beta_{max}]$ , and  $\Gamma = [\gamma_0, \gamma_{max}]$ , where  $\mathcal{T}, \mathcal{B}, \Gamma \subset \mathbb{R}_{>0}$ , letting  $N$  to be the only constant parameter.

The methodology setting is data-driven, i.e., we suppose to have the knowledge of a number of samples of the unknown solution, namely

$$\begin{aligned} \mathcal{X}_{tr} &= \{t_i^u; \beta_j^u, \gamma_k^u, \quad i = 1, \dots, N_t, j = 1, \dots, N_\beta, k = 1, \dots, N_\gamma\}, \\ \mathcal{Y}_{tr} &= \{y_i = u(t_i^u; \beta_j^u, \gamma_k^u), \quad i = 1, \dots, N_t, j = 1, \dots, N_\beta, k = 1, \dots, N_\gamma\}, \end{aligned} \quad (3)$$

where  $N_t, N_\beta$  and  $N_\gamma$  are the total number of sampled parameters  $t_i^u, \beta_j^u$  and  $\gamma_k^u$ , respectively.

Neural networks, in general, are trained in this type of training set, through an optimization algorithm aimed at minimizing a loss function, depending on the network parameters: the weights  $\omega$  and biases  $b$  [LeCun et al., 2015, Goodfellow et al., 2016]. In particular, PINNs use a model-dependent, customized loss to optimize network parameters. This loss integrates the governing equations of the ODEs System 2 while fitting the data, as follows [Raissi et al., 2019]:

$$\mathcal{L} = \mathcal{L}_{data} + \mathcal{L}_{ODE}. \quad (4)$$

To simplify the notation, in the following we omit the network parameters as well as the parameter  $\lambda \in \mathbb{R}_{>0}^3$ .

The two components of the loss function (4) are defined as follows:

$$\mathcal{L}_{data} = \text{MSE}(u_N, \mathcal{X}_{tr}, \mathcal{Y}_{tr}) \quad (5)$$

is the standard MSE loss, i.e., the approximation error computed considering the training dataset (3) of  $N_t \cdot N_\beta \cdot N_\gamma$  points.

On the other hand, the physics-endowed loss  $\mathcal{L}_{ODE}$  is the component that forces the neural network to approximate the known ODEs system structure. This is done by defining a so-called residual function,  $R(u, t; \lambda)$ , associated to the ODEs System 2, i.e.,

$$R(u, t; \lambda) := \frac{du(t; \lambda)}{dt} + F[u(t; \lambda); \lambda], \quad t \in [t_0, T], \quad \lambda \in \mathbb{R}_{>0}^3, \quad (6)$$

in such a way that the physics-endowed loss penalizes the solutions with a large residual, i.e.:

$$\mathcal{L}_{ODE} = \frac{1}{N_t^R \cdot N_\beta^R \cdot N_\gamma^R} \sum_{i,j,k} R(u_N, t_i^R; \beta_j^R, \gamma_k^R)^2, \quad (7)$$

where the points are taken in the so-called collocation set:

$$\mathcal{X}_{coll} = \{t_i^R; \beta_j^R, \gamma_k^R, \quad i = 1, \dots, N_t^R, j = 1, \dots, N_\beta^R, k = 1, \dots, N_\gamma^R\}. \quad (8)$$

The construction of this physics-informed loss function enables the addition of a regularization term that drives the network to learn the underlying model structure, simultaneously fitting the data, and preserving the initial conditions if they are specified. Compared to purely data-driven training, this mechanism allows us to benefit from one simple feedback neural network, with few layers and neurons, and to train it on small amounts of data [Raissi et al., 2019, Karniadakis et al., 2021].

## 2.2 Parameters inference

As a second step of our methodology, we employ an MCMC [Neal, 1993, Richey, 2010] method to extract, from a few noisy observations, the epidemic features that describe the underlined disease spreading process.

In particular, once our SIR-INN is trained on synthetic data close to real disease scenarios as described in Section 2.1, we use MCMC to estimate the epidemic parameters that drive the PINN solution to be as close as possible to the observations. We choose as fundamental parameters that characterize a disease spreading process the initial time of the spreading

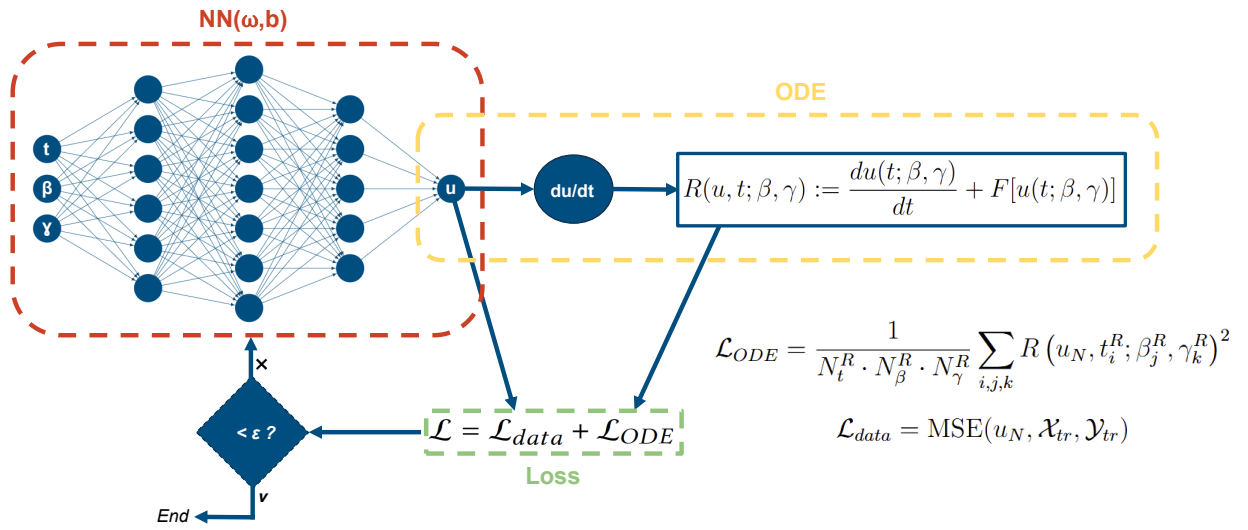


Figure 1: **Diagram of the PINN architecture for the SIR model learning.** The red-dashed frame represents the neural network which takes as inputs the time  $t \in \mathcal{T}$ , the disease transmission rate,  $\beta \in \mathcal{B}$ , the recovery rate,  $\gamma \in \Gamma$ , and outputs  $u \in \mathbb{R}^3$ , i.e., the three components of the SIR epidemic model: susceptibles, infectious, and recovered. Furthermore, the Neural Network (NN) is integrated with the physical knowledge of the SIR epidemic model, represented by the yellow-dashed frame, through the insertion of the ODEs system into the loss function of the NN, becoming a physics-informed neural network. PINN parameters, the weights  $\omega$  and biases  $b$ , are obtained by minimizing the total loss function, represented by the green-dashed frame, on the training data and satisfying a SIR-based dynamics as well.

process (i.e., the time at which we start to observe the data),  $t_0 \in \mathbb{R}_{\geq 0}$ , and the two transition rates of the SIR-based model, described in Section 2.1: the transmission rate and the removal rate,  $\beta \in \mathbb{R}_{\geq 0}$  and  $\gamma \in \mathbb{R}_{\geq 0}$ , respectively. Observe that at this stage the weights of the neural network are fixed, and the learned SIR-*INN* simply represents a function  $u_N^{\omega, b} : \mathcal{T} \times \mathcal{B} \times \Gamma \rightarrow \mathbb{R}^3$ . Then, the Markov chain Monte Carlo (MCMC) method is implemented assuming uniform distributions for all the parameters and the pre-trained PINN as the reference model. The model is fitted by minimizing the Mean Squared Error (MSE) between the model prediction and the observations, see also Equation 9 in the implementation details of Section 3.2.

Once we run the MCMC algorithm for a selected time window of observations, we obtain a Markov chain of the estimated parameters, from which we compute the mean values, namely:  $\hat{t}_0, \hat{\beta}, \hat{\gamma} \in \mathbb{R}_{\geq 0}$ .

## 2.3 Forecasting

The last step of our methodology is probably the most crucial but the simplest to implement and consists of forecasting the future state of the epidemic.

Suppose that for a fixed time window of observations we obtain the Markov chain of parameters that characterize the epidemic spreading dynamics exploited by the data, as described in Section 2.2. Then, first, we evaluate our reference model, the pre-trained SIR-*INN*, on the whole time window and on the estimated epidemic parameters:  $\hat{\beta}, \hat{\gamma} \in \mathbb{R}_{\geq 0}$ . Second, we consider as the mean model outcome the solution whose starting time point of the initial data in the observation time window corresponds to  $\hat{t}_0 \in \mathbb{R}_{\geq 0}$  estimated time. In this way, we obtain a mean model prediction for the entire time domain of the observation window and the forecasting window.

In the end, from a selected time window of observations, we are able to do short-term and long-term forecasting by simply evaluating our model on the estimated parameters and by considering a forecast time window of interest.

# 3 Implementation and evaluation details

All simulations were coded in the Python programming language using the following libraries: PyTorch version 2.0.1 [Paszke et al., 2019], Pymcmcstat package version 1.9.1 [Miles, 2019], seaborn library version 0.12.2 [Waskom, 2021]. Validation metrics were computed using the R programming language, specifically with the scoringutils package version 1.2.2 [Bosse et al., 2022].

## 3.1 PINN architecture and training details

Regarding the neural network architecture, we leverage the regularization mechanism of the PINNs to benefit from simple feedforward neural networks, minimizing as much as possible the computational cost derived by the usual deep neural networks [Raissi et al., 2019, Karniadakis et al., 2021]. We implemented a single PINN consisting of only three hidden layers, and an overall architecture of  $[3, 16, 32, 16, 3]$ , where each value denotes the number of neurons per layer, from input to output. As activation functions, we use smooth differentiable

functions, commonly used for PINNs [Cuomo et al., 2022]: hyperbolic tangent for the hidden layers and sigmoid activation function for the output layer, to have outputs in the range  $[0, 1]$ .

As described in Section 2.1, to train our SIR-INN, we chose synthetic data for the training set and the collocation set. In particular, since we generated them to construct the training set (3), we used the same samples for the collocation set (8), hence, following the same notation of Section 2.1, we considered  $\mathcal{X}_{tr} \equiv \mathcal{X}_{coll}$ . For the time component,  $t_i^u$ , we used weekly time data in a time window of 600 days; from  $t_1^u = 0$  to  $t_{86}^u = 595$ . Regarding the ranges of parameters, we, firstly, select a uniform grid of size 50 considering the removal rate  $\gamma \in [1/12, 1/2.5]$ , and the transmission rate  $\beta \in [0.12, 0.45]$ . Then we restricted the values with linear constraints around the diagonal of the grid (that is, around  $R_0 = \beta/\gamma = 1$ ) obtaining 1068 pairs of values  $(\beta_j^u, \gamma_k^u)$ ,  $j = 1, \dots, N_\beta$ ,  $k = 1, \dots, N_\gamma$ , where  $N_\beta \cdot N_\gamma = 1068$ , for which the supposed mean infective period,  $1/\gamma$ , lasts from 2 to 12 days and  $R_0 \in (0.75, 2.5)$ . To construct the  $\mathcal{Y}_{tr}$  training set (3), for each pair of parameters,  $(\beta_j^u, \gamma_k^u)$ , we first generated the solutions  $u(t_i^u; \beta_j^u, \gamma_k^u)$  (i.e., the SIR components) via *odeint*. This is done considering the whole daily time window of 600 days for  $t_i^u$ , the population size  $N = 1e^6$ , and the SIR initial conditions:  $(S(0), I(0), R(0)) = (N - 1, 1, 0)$ . Second, we restricted the generated samples to the weekly time window, coherently with the  $\mathcal{X}_{tr}$  training set (3). All of these parameters and synthetic data choices are decided according to possible seasonal influenza scenarios, while trying to generalize them to better train our neural network, increasing its generalization capabilities.

The PINN is trained for 7500 epochs using the Adamax optimization algorithm, with a learning rate of 0.001. We train the NN with the same batches of 100 training, validation and collocation points, with train size = 0.9 .

## 3.2 Parameters inference details

As explained in Section 2.2, for the parameter estimations we leverage an MCMC method whose loss function is a MSE, namely, between a function  $g$  of the data and a function  $G$  of the PINN output (i.e., in terms of the SIR model components), as follows:

$$\mathcal{L}(t_0, \beta, \gamma) = \frac{1}{M} \sum_{j=1}^M \|G(u_N(t_j, \beta, \gamma)) - g(t_j, \bar{t}_0, \bar{\beta}, \bar{\gamma})\|_2^2. \quad (9)$$

In this way, we are considering a time window of  $M$  observations, each at time  $t_j \in \mathbb{R}_{\geq 0}$ , from which we infer the parameters  $(\bar{t}_0, \bar{\beta}, \bar{\gamma}) \in \mathbb{R}_{\geq 0}^3$  that characterize the hidden function of data.

Furthermore, since data can be provided as Influenza-Like-Illness (ILI) incidence observations, instead of the number of infectious reported cases, we defined the function  $G$  of our PINN solution coherent with the function that represents the data,  $g$ . Hence, since incidence is calculated as reported infectious cases per 1000 patients, we assume  $g(t, \bar{\beta}, \bar{\gamma}) := -\frac{dS(t)}{t} \cdot \frac{1000}{N}$ . This means that ILI incidence observations are represented by the opposite normalized difference of susceptible individuals. In this way,  $G$  evaluated in one fixed tuple of parameters can be written as follows:

$$G(u_N(t_j, \bar{\beta}, \bar{\gamma})) := \{u_N(t_{j-1}, \bar{\beta}, \bar{\gamma})[0] - u_N(t_j, \bar{\beta}, \bar{\gamma})[0]\} \cdot 1000. \quad (10)$$

Then the MCMC method is executed for a selected time window of observations, for the 10,000 simulations. The values of the initial parameters are  $(t_0, \beta, \gamma)|_{iteration=0} = (200, 0.2, 0.15)$ , with lower and upper bounds for each parameter, respectively:  $\hat{t}_0 \in [0, 400]$ ,  $\hat{\beta} = [0.12, 0.45]$  and  $\hat{\gamma} = [1/12, 1/2.5]$ . From the Markov chain obtained from each run of the MCMC algorithm, we compute the mean values of the distribution tails,  $\hat{t}_0, \hat{\beta}, \hat{\gamma} \in \mathbb{R}_{\geq 0}$ , as the last 5000 of the chain samples.

### 3.3 Epidemiological data

We used seasonal influenza national data provided by the Italian National Institute of Health (ISS) [[Istituto Superiore di Sanità, 2020](#)] through the RespiVirNet surveillance system. These consist of weekly Influenza-Like-Illness (ILI) incidence observations reported by sentinel doctors at both national and regional levels (with the exception of the Valle d’Aosta and Calabria regions for the season 2023-2024), starting from the season 2003-2004 to the most recent, 2024-2025. In particular, we perform simulations for both the seasons 2023-2024 and 2024-2025, with influenza surveillance running from November to May, starting from week 42 in a given year and continuing until week 17 of the following year.

All data is publicly available on GitHub at: [RespiVirNet, 2020 \[2020\]](#).

### 3.4 Forecasting evaluation metrics

We evaluate our SIR-INN framework forecasting performances using several metrics, employed and described in detail in [Fiandrino et al. \[2025\]](#).

**Absolute Error (AE).** It is computed as the absolute value of the difference between the median forecast and the actual corresponding value. The mean absolute error (MAE) is the average of the AE over different time steps. We also implemented it by averaging for all the forecasting time windows.

**Weighted Interval Score (WIS).** It is an approximation of the Continuous Ranked Probability Score (CRPS) [[Bracher et al., 2021](#)] that evaluates both the accuracy of the forecast median solution and of the prediction intervals in containing the actual observations. The metric is defined for a given prediction interval of a model forecast, generalizing the interval score to multiple prediction intervals. In particular, we considered  $K = 11$  prediction intervals defined by  $\alpha_K = 0.02, 0.05, 0.10, 0.20, 0.30, 0.40, 0.50, 0.60, 0.70, 0.80, 0.90$ . For the non-negative weights assigned to the different intervals, we set  $w_0 = 1/2$  and  $w_K = \alpha_K/2$ .

**Coverage.** It measures the calibration of a model and is defined as the fraction of times a prediction interval contains the actual data. Notice that in a well-calibrated model, the coverage values should closely match the nominal levels of the predictive intervals. For example, observations will be included exactly 90% of the time in the prediction interval 90%. We also computed the coverage for both the 50% and 90% prediction intervals of our forecasts.

## 4 Results

We demonstrate the relevance of our methodology to disease forecasting using national data from Italian seasonal influenza, provided by the Italian National Institute of Health (ISS) [Istituto Superiore di Sanità, 2020], as a representative real-world epidemic scenario. In particular, to increase both the complexity and the relevance of the task, we put ourselves under the same conditions as the teams that participated in the Influcast Hub challenge 2023-2024 [InfluCast, 2025]. Specifically, we perform four weeks ahead forecasting simulations, as outlined in Section 4.2.1, and we employ the same validation metrics adopted in Fiandrino et al. [2025] to ensure a fair comparison between our model and all the models of the participating teams. For the corresponding quantitative results, we refer to Section 4.2.2. Moreover, in Section 4.1 we show the results on parameter inference obtained by our model using a methodology MCMC. In addition, in Section 4.2.3 we analyze the performance of our approach also in long-term forecasting of seasonal influenza. All experiments were carried out using data from two different influenza seasons (years 2023-2024 and 2024-2025), to illustrate the ability of our SIR-INN hybrid methodology to generalize across different epidemic scenarios without retraining the neural network.

### 4.1 Parameters inference results

As explained in Section 3.2, after we have selected an ideal size for the observation time window,  $M = 5$  (see also Equation 9), we perform an MCMC simulation every time we observe new data. For example, at week 51, we use five data points of the weeks 47-51, to estimate the parameters that best align the SIR-based PINN output to the observed ILI incidence in this window. In line with the Influcast Hub, we performed simulations starting with four weeks of observation (also for the 2023-2024 influenza season) and considering retrospective weekly updates of past observations, as the system provides new surveillance data. In the end, the total number of simulations is equal to the number of total observations (i.e., the total number of weeks in a season) minus four, which is 24 for both seasons. Note that for the first simulation we used only four observations, as they are the only available ones.

Figure 2 shows the mean values of the estimated parameters  $\hat{t}_0, \hat{\beta}, \hat{\gamma} \in \mathbb{R}_{\geq 0}$  and the expected values of  $\hat{R}_0 = \frac{\hat{\beta}}{\hat{\gamma}}$  for all simulations (that is, weeks), for the season 2023-2024 (Figure 2a) and 2024-2025 (Figure 2b). From the plots, we observe that the mean values of the estimated parameters are similar across the two considered seasons, and their values remained stable as the seasons progressed. The average disease transmission rate,  $\beta$ , and the removal rate,  $\gamma$ , are close to 0.3, leading to an average  $R_0$  equal to 1.14 in both cases. Regarding the initial spread time,  $t_0$ , its average throughout the weeks is close to day 300, corresponding to the end of October, both for the 2023-2024 and 2024-2025 seasons.

Even if the best parameters' values are re-estimated every week, as new surveillance data are reported and previously published data are updated, our model consistently identifies a narrow range of plausible values that remain almost constant across the season. The largest fluctuations are observed for the estimated  $\hat{t}_0$ , which the model adjusts to capture the temporal dynamics of the outbreak, which was different in the two seasons. While in 2023-2024 the ILI incidence peaked at weeks 51-52, in 2024-2025 the peak arrived a month

later, at weeks 4 and 5.

Interestingly, the estimated values of  $\beta$  and  $\gamma$  are in line with the typical values measured for seasonal influenza. In particular, an average infectious period of about 4 days ( $\hat{\gamma} = 0.25$ ), and a basic reproductive number of  $R_0 \sim 1.2$  correspond to the traditional estimates of these parameters for seasonal flu [Carpat et al., 2008, Biggerstaff et al., 2014]. Thus, although this is not explicitly enforced, we see that the data and the structure based on SIR allow the model to effectively learn the epidemiological role of the two parameters,  $\beta$  and  $\gamma$ .

## 4.2 Forecasting results

Here we show the performance of our SIR-INN both on short-term and long-term forecasting, as described in Section 2.3.

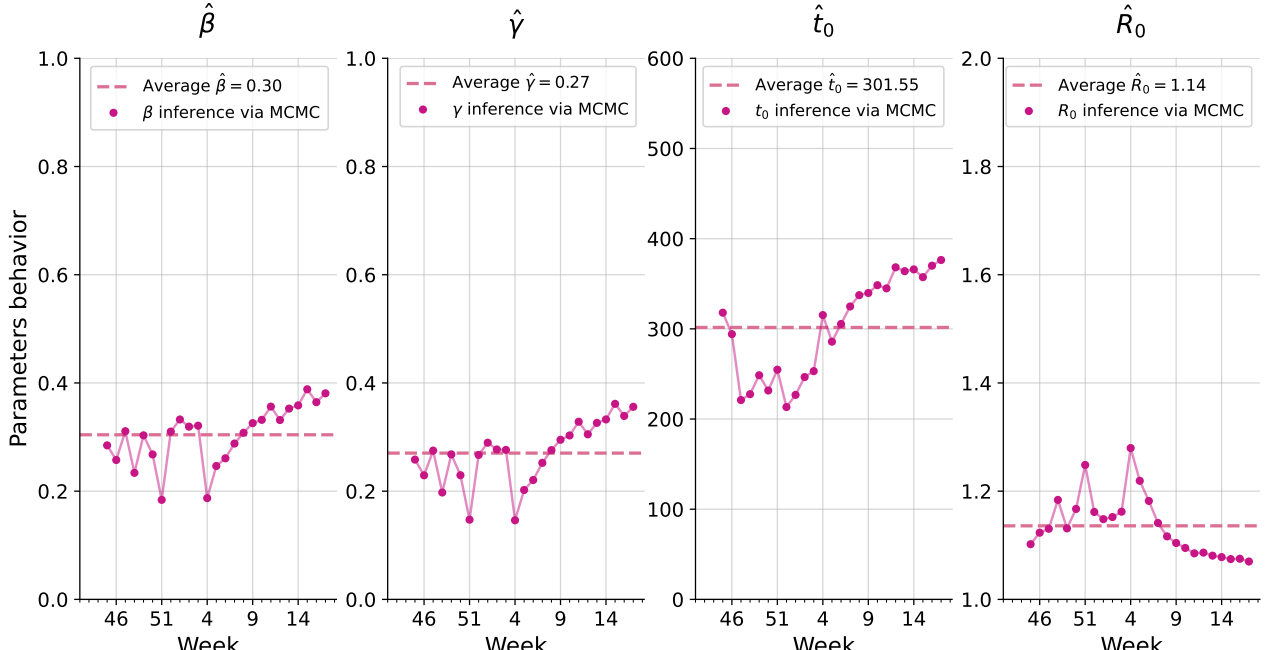
From the results derived from the estimation of the parameters via MCMC, we obtain Markov chains referred to each time window of observations, and the mean values of the relative parameters, namely  $\hat{t}_0, \hat{\beta}, \hat{\gamma} \in \mathbb{R}_{\geq 0}$ . Hence, we perform probabilistic forecasting in the form of quantiles with prediction intervals based on model outcomes, on each evaluation window, defined as the union of the observations time window and the forecast time window. In particular, for each MCMC chain we select 500 random samples to draw from the posterior, then we evaluate our model on these samples, computing the quantiles as measures of uncertainty.

### 4.2.1 Four-weeks-ahead forecasting

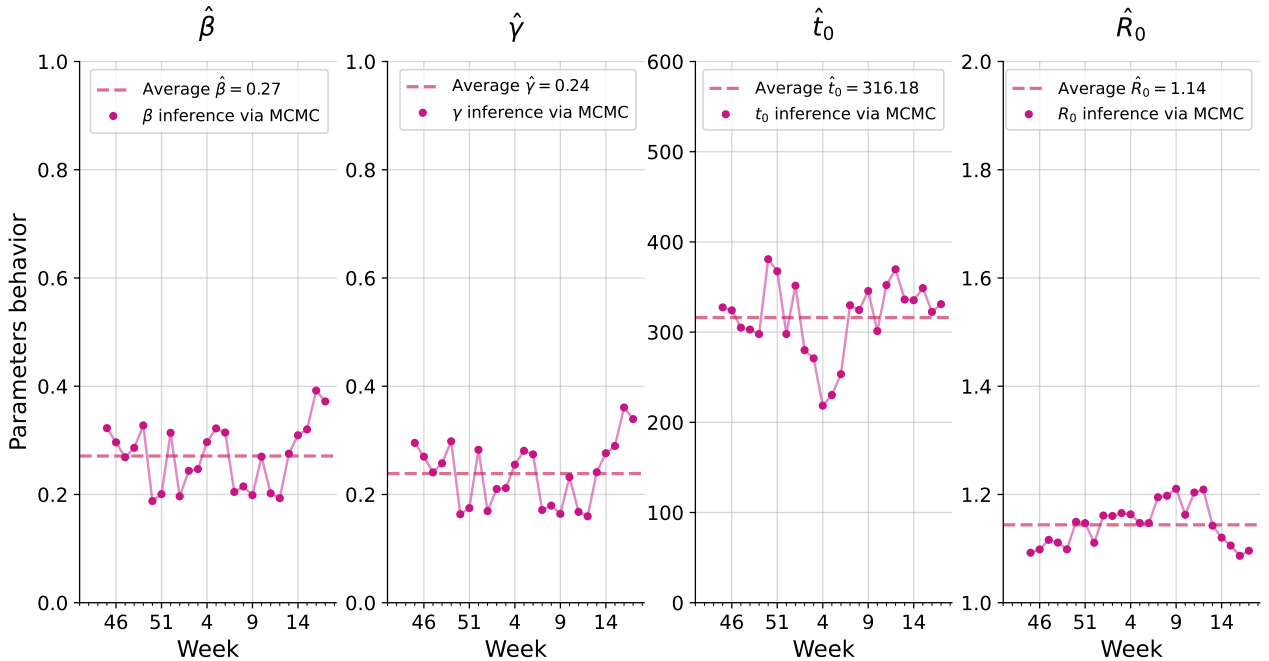
As the first set of experiments, we generate forecasts four weeks ahead, according to the Influcast Hub forecasting standards [InfluCast, 2025]. This means that, similarly to the parameter inference experiments, we update our forecasts each time the epidemic curve is updated with a new observation, removing the oldest one within a time window of five data points. We consider a fixed size of four weeks for the forecast time window. Note that for the last four simulations, we forecast on a shorter time window since we do not have other future observations to compare with.

Figures 3 and 4 show the results for nine representative time windows and for the 2023-2024 and 2024-2025 seasons, respectively. Note that the error bars and the mean results of SIR-INN start from the last reported incidence observation, since our methodology based on PINN produces uncertainty throughout the evaluation window. The complete results obtained considering all the time windows are shown in 6, Figure 6, for the 2023-2024 season, and in Figure 7, for the 2024-2025 season.

In the 2023-2024 influenza season (Figure 3), we can see that SIR-INN is fairly accurate in the initial phase of the outbreak, despite the inherent challenges associated with the limited number of observations available at that stage. However, the forecast tends to underestimate the observed incidence in this initial period, as shown by the forecasts at weeks 46, and 48. As the peak time approaches, in weeks 51 and 52, we can see that the error bars become larger, and the 90% percentile interval contains the current data and almost all of the following four observations. In particular, the model correctly identifies the occurrence of the peak, which is the most critical and challenging phase, even if the actual incidence value is slightly overestimated. The declining epidemic phase that follows the peak is well predicted by SIR-



(a)



(b)

Figure 2: **Behavior of the SIR-based model parameters estimated via MCMC.** At each week we consider the observations time window of size 5 which includes the previous four weeks and the current one. The inferred features represented in the figure are, respectively, the transmission rate, the recovery rate, the initial time of the spreading, and the basic reproduction number. The pink dashed lines indicate the average value across the individual weekly values of the inferred parameters. National data used are from seasonal influenza of (a) 2023-2024, and (b) 2024-2025.

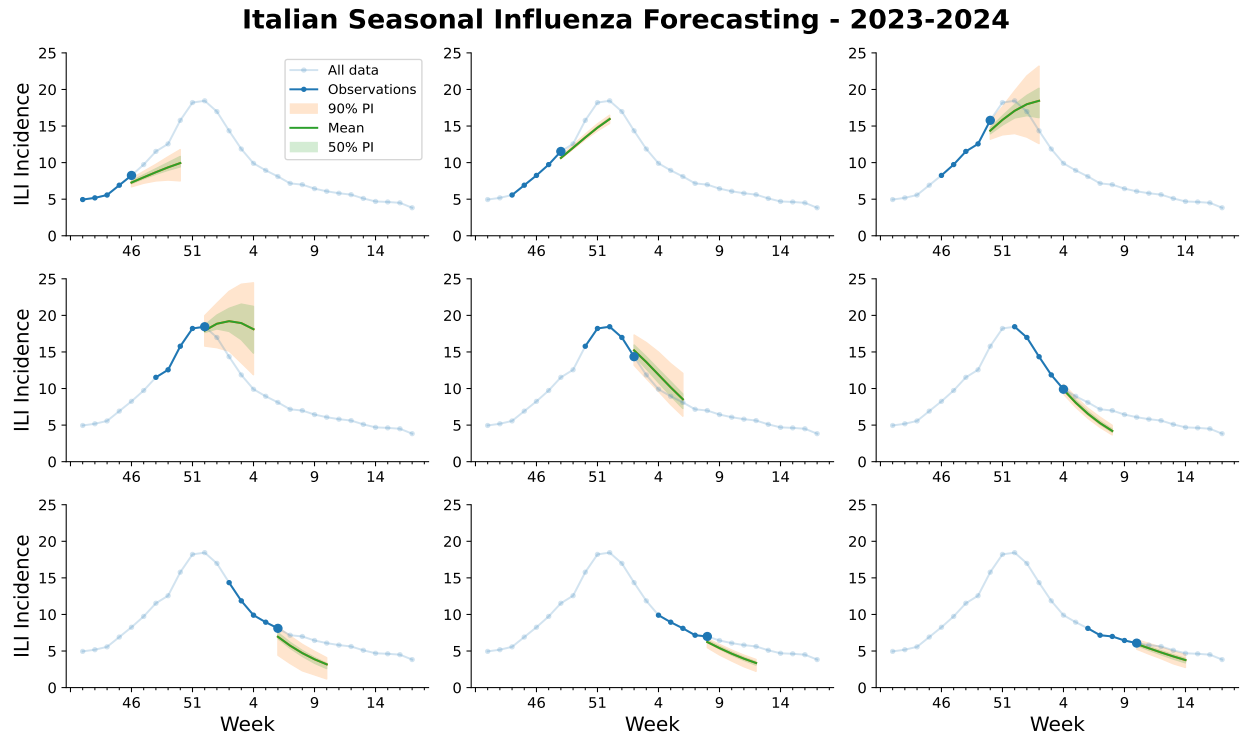


Figure 3: **Seasonal influenza forecasting four weeks ahead via SIR-INN.** The ground truth data, in blue, represent the weekly observations at national level of the 2023-2024 seasonal influenza. The highlighted blue data represent the time window of observations, with fixed length of 5, from which the SIR-based PINN infers the epidemic parameters and then forecasts on the following four weeks ahead. The mean-model forecasts are represented with green lines and the 50% and 90% percentile intervals are shaded, respectively, in green and orange error bars.

### Italian Seasonal Influenza Long-Term Forecasting - 2024-2025

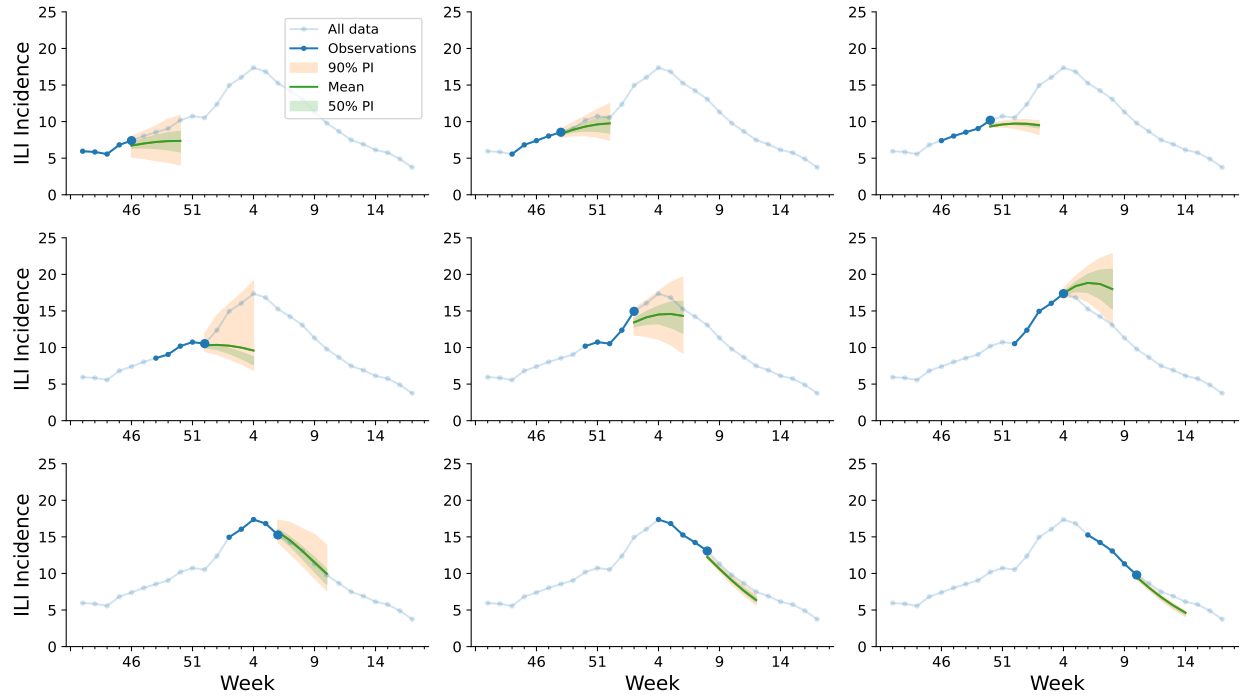


Figure 4: **Seasonal influenza forecasting four weeks ahead via SIR-INN.** The ground truth data, in blue, represent the weekly observations at national level of the 2024-2025 seasonal influenza. The highlighted blue data represent the time window of observations, with fixed length of 5, from which the SIR-based PINN infers the epidemic parameters and then forecasts on the following four weeks ahead. The mean-model forecasts are represented with green lines and the 50% and 90% percentile intervals are shaded, respectively, in green and orange error bars.

INN, in its initial phase (weeks 3 and 4). However, as the outbreak fades out, our model rapidly begins to underestimate the real observations, forecasting a rapid extinction of the new reported cases. The forecasting accuracy increases again in the final part of the season, as the curve approaches the baseline values again (weeks 10-14).

The results for the 2024-2025 season (Figure 4) show an increased accuracy of forecasting, compared to the previous year. The early outbreak phase, the peak time, and the decreasing phase are consistently estimated with good accuracy. In particular, the crucial forecast of peak time is improved with respect to the results of the 2023-2024 season. The peak incidence time and the prediction of peak ILI incidence are close to the real ones. The peak incidence is slightly underestimated when projected from week 2, and slightly overestimated at week 4. The predicted peak time in both cases is nearly identical to the real one, and the general trend is well captured by our model. However, at week 50, we can see that our model is unable to accurately predict the later increase in the ILI incidence curve. In fact, this challenging prediction is still in line with most of the forecasts reported on the Influcast platform [[InfluCast, 2025](#)]. Instead, by week 52, the model appears surprisingly to infer that the current peak may represent only a relative infection peak, thus anticipating a potential subsequent rapid increase in incidence. As shown by the forecast for week 52, even if the predicted mean and the 50% percentile interval incorrectly display a trend of decreasing incidence, the 90% percentile interval contains all observations. Note that the mean outcome of SIR-INN in this case seems to converge to the observations, deviating from the 50% percentile interval. This is because our methodology produces a mean forecast that is different from the forecast median and hence can fall outside the error bars. Finally, our model effectively captures the decreasing phase of the outbreak. This clearly emerges from the forecasts at weeks 6 and 8 where the SIR-INN mean forecast, represented by the green line, almost perfectly fits the unseen observations and the 50% percentile intervals contain almost all the data. Only the latest observations are slightly underestimated by our model forecasts, as shown by the results of week 10.

Table 1 describes the forecast performance of our model compared to the baseline, used as a reference model in [Fiandrino et al. \[2025\]](#), for both influenza seasons. The results are obtained from national-level four-weeks-ahead forecasting using several metrics, aggregating forecasts from all rounds and all the horizons. The number of rounds represents the number of simulations considered for evaluation. In line with the Influcast hub challenge [[InfluCast, 2025](#)], we considered a total number of 20 rounds for the 2023-2024 season, starting the first four-weeks-ahead forecasting from the 46th week of 2023 and finishing with the last forecast simulation at week 13th of 2024. For the season 2024-2025, we started to evaluate the performances of the simulation whose last observation corresponds to the 45th week of 2024. The number of horizons considered for the evaluation is four, corresponding to the size of the forecast time window. A detailed description of the evaluation metrics is reported in Section 3.4.

From the results shown in Table 1 we can see that, in both seasons, SIR-INN consistently outperforms the baseline in terms of point forecast accuracy, as confirmed by lower MAE and WIS values. Specifically, the MAE of the median forecast decreases from 2.68 to 2.31 in 2023-2024 and from 2.54 to 1.87 in 2024-2025, corresponding to improvements of approximately 14% and 26%, respectively. A similar trend is observed for WIS, with reductions of 12% and 21%. As we previously noted in the incidence plots, a substantial improvement in forecast

Model	Influenza Season	N. of Rounds	MAE	WIS	Coverage 50%	Coverage 90%
Baseline	2023/2024	20	2.68	1.90	<b>0.49</b>	<b>0.66</b>
SIR-INN	2023/2024	20	<b>2.31</b>	<b>1.68</b>	0.08	0.34
Baseline	2024/2025	21	2.54	1.71	0.14	<b>0.52</b>
SIR-INN	2024/2025	21	<b>1.87</b>	<b>1.35</b>	<b>0.21</b>	0.51

Table 1: **Forecasting performance of the SIR-INN model, compared to the baseline.** The results are obtained from the four-weeks-ahead forecasting at national level, across the two influenza seasons, in terms of Mean Absolute Error (MAE) of the median forecast, Weighted Interval Score (WIS), 50% and 90% coverage. Bold values indicate the best performance for each metric within the corresponding season.

precision is observed for the 2024–2025 season compared to 2023–2024. Both the MAE of the median forecast and the WIS values are notably lower, meaning that the accuracy of the median forecast and the prediction intervals in bounding the actual observations is greater for the 2024–2025 season relative to the previous one. Moreover, although the coverage values remain somewhat below the ideal nominal levels, their increase suggests that the model exhibited an improved calibration by passing from the previous influenza season to the most recent.

#### 4.2.2 Comparison with Influcast models

Since we performed four-week forecast simulations of Italian seasonal influenza 2023–2024 according to the requirements of the Influcast challenge [InfluCast, 2025], we implemented the same validation metrics adopted in Fiandrino et al. [2025] to evaluate the accuracy of our model relative to those of the other teams. Table 2 presents the aggregated performance, for all rounds and horizons, of all models under consideration, as in Fiandrino et al. [2025], with the addition of our model’s performance (last row). Regarding the performance evaluation of all the Influcast models, the relative values of the MAE of the median forecast and the WIS are computed by comparing pairs of models that participate in the same forecast round. These values are then normalized by dividing by the corresponding value of the baseline model. In addition, these values incorporate both national-level seasonal influenza predictions and aggregated regional forecasts, in contrast to national-level results reported in Section 4.2.1. In this way, each individual model’s result accounts for both regional and national aggregated outcomes of all other models, and it is expressed relative to the baseline. Consequently, relative values below 1 indicate better performance than the baseline, while values above 1 indicate worse performance. The ensemble model is obtained by combining all the model forecasts, and it consistently outperforms the baseline model on all results, as detailed in Fiandrino et al. [2025], which also provides further information on the single models and evaluation metrics. Regarding our model results, the relative MAE of the median forecast and the WIS are computed by comparison with the results of all other models and normalized by the corresponding baseline values. Note that SIR-INN’s relative results are evaluated with respect to the other models, whereas the reverse does not hold, as we did not officially participate in the challenge. Consequently, the ensemble model also does not include our model’s predictions. Moreover, the values related to our model are all derived from national-

Model	N. of Rounds	Relative MAE	Relative WIS	Coverage 50%	Coverage 90%
Mechanistic-1	19	0.56 (1st)	0.54 (1st)	0.75	0.89 (1st)
Mechanistic-2	20	1.86	1.64	0.04	0.49
Mechanistic-3	20	0.58 (2nd)	0.58 (3rd)	0.47 (3rd)	0.70 (3rd)
Mechanistic-4	19	0.73	0.73	0.16	0.37
Semi-mechanistic-1	16	1.80	2.14	0.06	0.27
Semi-mechanistic-2	14	0.84	1.04	0.19	0.30
Statistical-1	20	0.99	1.09	0.17	0.43
Statistical-2	19	0.77	0.85	0.11	0.31
Ensemble	20	0.59 (3rd)	0.57 (2nd)	0.51 (1st)	0.80 (2nd)
Baseline	20	1.00	1.00	0.49 (2nd)	0.66
SIR-INN	20	1.04	1.03	0.08	0.34

Table 2: **Forecasting performance of the SIR-INN model compared to Influcast models.** The results are obtained from the four-weeks-ahead forecasting at national level in terms of relative Mean Absolute Error (MAE) of the median forecast, relative Weighted Interval Score (WIS), 50% and 90% coverage.

level predictions, rather than regional ones.

Taking into account the results of our model, outlined in the last row of Table 2, the relative MAE and WIS values are slightly worse than the baseline (1.04 and 1.03, respectively), yet the overall performance remains comparable to that of the other models. Specifically, in terms of relative MAE, our model outperforms two other models: *Mechanistic-2* (1.86) and *Semi-mechanistic-1* (1.80), while it notably ranks fifth in terms of relative WIS, ahead of *Semi-mechanistic-1* (2.14), *Mechanistic-2* (1.64), *Statistical-1* (1.09), and *Semi-mechanistic-2* (1.04). In terms of coverage, although the values are below the ideal nominal levels, our model still compares well with the others. It performs better than *Mechanistic-2* (0.04) and *Semi-mechanistic-1* (0.06), for the coverage 50%, and outperforms three models, *Semi-mechanistic-1* (0.27), *Semi-mechanistic-2* (0.30), and *Statistical-2* (0.31), for the coverage 90%. In summary, our model shows overall performance in line with the participating Influcast models [InfluCast, 2025], usually ranking above the bottom three. This suggests that its implementation could positively contribute to the prediction of future seasonal influenza epidemics, when included in the ensemble forecasts.

#### 4.2.3 Ten-weeks-ahead forecasting

In addition, we analyze the performances of our SIR-INN also on long-term forecasting. The experimental setup is identical to the one implemented for the short-term forecasts, with the only difference being a different size for the forecasting time window. In this case, we select a range of ten weeks instead of four weeks.

The results for the 2023-2024 season obtained considering four consecutive time windows of observations that precede the peak phase are shown in Figure 5. For the results of the 2024-2025 season, see Figure 8, in 6.

The results of the 2023-2024 influenza season, shown in Figure 5, illustrate how our model, starting from only a few initial observations, is able to partially capture the epidemic trend beyond the short-term horizon, although without providing a fully accurate estimate. In

## Italian Seasonal Influenza Long-Term Forecasting - 2023-2024

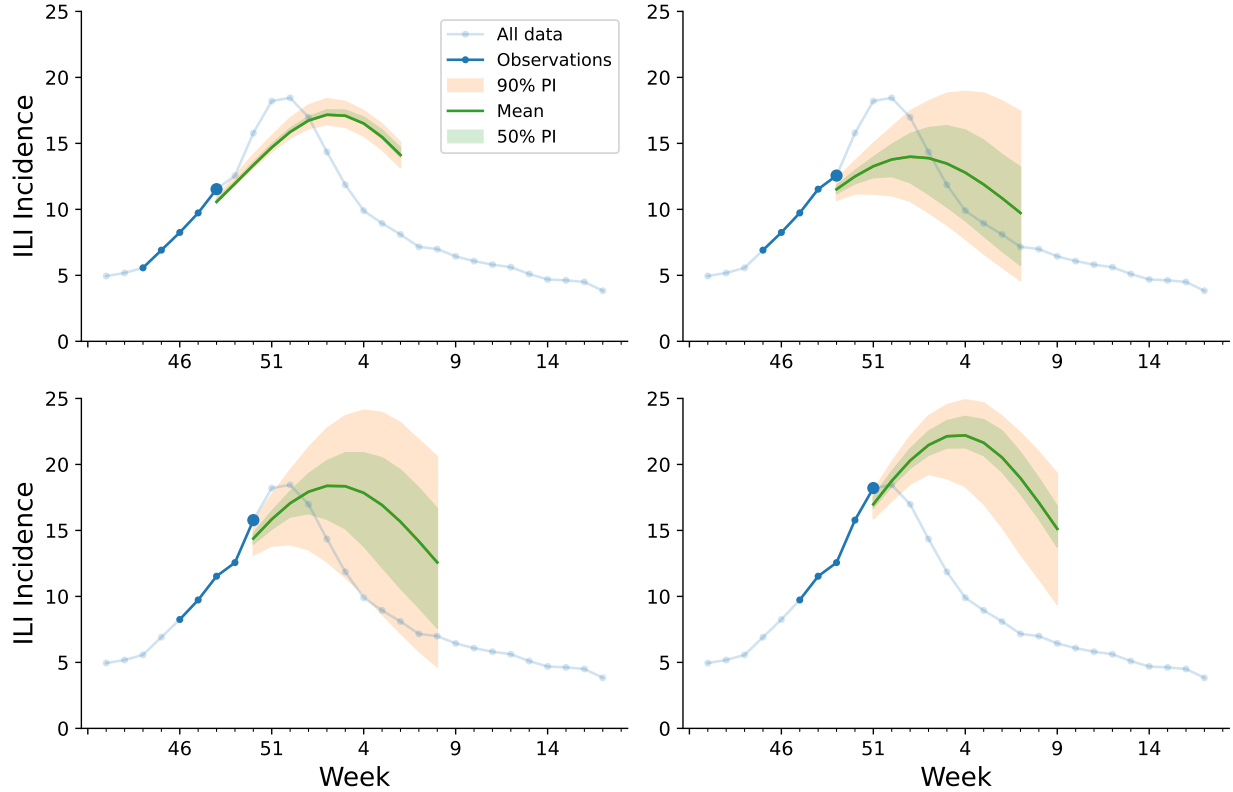


Figure 5: **Seasonal influenza forecasting ten weeks ahead via SIR-INN.** The ground truth data, in blue, represent the weekly observations at national level of the 2023-2024 seasonal influenza. The highlighted blue data represent the time window of observations, with fixed length of 5, from which the SIR-based PINN infers the epidemic parameters and then forecasts on the following ten weeks ahead. The mean-model forecasts are represented with green lines and the 50% and 90% percentile intervals are shaded, respectively, in green and orange error bars.

all scenarios depicted in Figure 5, the forecast curve exhibits a broader shape relative to the curve derived from interpolated observations, tending to underestimate the data points before the peak and, conversely, overestimate the observations once the peak has passed. The peak time is consistently predicted later than the actual one, although the discrepancy remains within a maximum of four weeks. The model tends to underestimate the peak ILI incidence of the data in many cases, and in the last scenario the model overestimates it.

Although the influenza season is still at an early stage and only few observations are available, in the first panel we can observe that the mean-model prediction is reliable. Although the error bars are very narrow, the overall trend of the mean model, as well as the peak incidence ILI, appears to be well forecast. A particularly interesting result is shown at week 50, where the model mean forecast, represented by the green line, as well as the peak estimation, are reasonably accurate, and almost all ten unknown observations fall within the 90% percentile interval.

Even in the case of long-term forecasting, the results, presented in 6, Figure 8, are more promising for the 2024–2025 season than the 2023–2024 one. The 90% prediction interval contains almost all observations for the pre-peak scenarios, even at week 52 when a first, minor peak of infections occurred. In addition, the model’s ability to predict the maximum ILI incidence increases as the epidemic peak approaches.

## 5 Discussion

In this work, we have introduced a novel framework for epidemic forecasting, namely SIR-INN, based on Physics-Informed Neural Networks (PINNs). Specifically, we endowed a single neural network with a prior epidemiological knowledge leveraging the well-known Susceptible-Infectious-Recovered (SIR) compartmental model, with constant transition rates. The neural network has been trained only once on temporal-epidemic domains close to real epidemic scenarios. In this way, starting from a limited set of noisy observations, our PINN is able to infer, via Markov chain Monte Carlo (MCMC), the parameters that characterize a SIR-based epidemic dynamics. Following this inference step, we used our PINN to forecast the dynamics of epidemics in future time windows.

We used national data from the Italian seasonal influenza surveillance, provided by the Italian National Institute of Health (ISS) [Istituto Superiore di Sanità, 2020], as done by previous studies on influenza forecasting [Zhang et al., 2015, Perrotta et al., 2017, Brownstein et al., 2017]. Our results obtained from a direct application of the framework to national data of the influenza seasons 2023-2024 and 2024-2025 confirm the good forecasting abilities of our hybrid methodology.

Despite differences in weekly observations and predictions of associated parameters, our results indicate that both seasonal influenza outbreaks showed similar epidemiological characteristics in terms of transmissibility and average infectious period. Such epidemiological features are shown to be underpinned by a piecewise constant SIR model, with disease transmission rate and removal rate values close to 0.3 and an average basic reproduction number  $R_0$  of approximately 1.14.

We then performed four-weeks-ahead forecasting simulations based on inferred parameters employing the same validation metrics adopted by Fiandrino et al. [2025]. From the

qualitative results, we can see that for the 2023-2024 influenza season, and especially for the 2024-2025 season, the mean forecasting solutions during the early period and the decreasing stage are often fairly accurate. This is particularly relevant considering that providing accurate forecasts during the early phase of an outbreak is challenging, primarily due to the limited number of available observations, which are often noisy. Even more challenging is the estimation of the incidence peak. Although the model does not achieve high accuracy in forecasting the season peak, it appears to anticipate its occurrence reasonably well. Specifically, for the 2024-2025 influenza season, the model appears to have identified, with a non-negligible probability, that the peak in week 51 did not correspond to the actual peak of the epidemic. In general, Figures 3 and Figure 4 suggest that our model is more effective in capturing the temporal pattern of the influenza season 2024-2025. This impression is also confirmed by the results in Table 1, which report the Mean Absolute Error (MAE) of the median forecast, Weighted Interval Score (WIS), and 50% and 90% coverage for both seasons. In general, our SIR-INN framework appears to outperform the baseline, used as a reference model in [Fiandrino et al. \[2025\]](#), particularly in terms of MAE and WIS. This makes our model a possible competitive alternative to the baseline for seasonal influenza forecasting. These findings are also supported by the results of the seasonal influenza forecast for 2023-2024 presented in Table 2, where all models participating in the Influcast four weeks ahead forecast challenge [[InfluCast, 2025](#)] were compared to ours. These results show that the performances of our model are comparable to those of current state-of-the-art models. In particular, the SIR-INN performs better in terms of the relative WIS, thereby demonstrating the accuracy of the prediction with respect not only to the median outcome but also to the prediction intervals. In summary, these results suggest that our framework could meaningfully enhance the forecasting of successive seasonal influenza epidemics, increasing the ensemble's predictive performance.

In addition, in Section 4.2.3, we analyze the performance of our model in long-term forecasting, specifically ten weeks in advance. In Figure 5, we can see that although the influenza season is still in an early stage and only a few observations are available, our model is able to partially capture the epidemic trend. This is particularly relevant considering that long-term forecasting often fails when using fully data-driven and neural network-based approaches [[Rodríguez et al., 2024](#), [Ye et al., 2025](#)].

Together, these findings align with what is increasingly emphasized in the forecast epidemiology literature. Adopting a hybrid approach that integrates the mechanistic understanding of disease transmission with the learning and generalization capabilities of neural networks appears to be a promising direction to improve forecast performance [[Rodríguez et al., 2024](#), [Ye et al., 2025](#)]. The developed framework allows us to benefit from both approaches, thus maximizing forecasting capabilities in both short-term and long-term predictions. On the one hand, to preserve the underlying dynamic structure of influenza transmission, we use the simplicity of the SIR model, supported by theoretical studies, with fixed epidemiological parameters. On the other hand, the neural network component allows us to exploit data-driven patterns, improving the flexibility and generalization ability of the model [[Raissi et al., 2019](#), [Rodríguez et al., 2024](#)]. Furthermore, we take additional advantage of the hybrid nature of the framework by implementing an MCMC method, separately from the neural network, to automatically capture the temporal variability of the SIR parameters. Our results suggest that even complex epidemic dynamics may reflect a simple, shared

mathematical structure that deserves consideration in purely ML-based forecasting models [Ye et al., 2025].

The resulting framework, despite the combination of diverse and potentially complex hybrid components, remarkably preserves simplicity, explainability, efficiency, and cost-effectiveness. Our SIR-INN consists of a single neural network trained only once on synthetic data, in contrast to the majority of machine learning (and hybrid) approaches for epidemics forecasting [Kharazmi et al., 2021, Rodríguez et al., 2023, Millevoi et al., 2024]. This makes the method highly flexible and generalizable. The neural network does not require retraining each time a new observation is available or when a new influenza season occurs. SIR-INN framework also allows us to obtain parameter distributions independently of the neural network train, thereby eliminating the need for retraining it while allowing for the quantification of forecast uncertainty. Performing Uncertainty Quantification (UQ) is essential in epidemiological forecasting, as it contributes to model robustness and supports more reliable decision-making in public health. Given the inherent variability and noise of epidemiological data, capturing forecast uncertainty is necessary to avoid overconfidence and misinterpretation of the model output [Funk et al., 2019, Bracher et al., 2021, Sherratt et al., 2023]. However, in neural network-based approaches where the output is a single trajectory, incorporating this uncertainty remains challenging and is therefore still rarely implemented in the current literature [Linka et al., 2022, Shi et al., 2025]. Our work can be seen as an initial and promising attempt toward incorporating uncertainty into forecasting within this class of hybrid approaches. However, as the results suggest, further work is still needed in this direction. The model occasionally exhibits overconfidence, resulting in overly tight percentile intervals and consequently underperforming in terms of coverage. This behavior occurs mainly during the early or late phases of the outbreak, while the prediction of peak time and peak incidence is associated with greater uncertainty, ensuring greater reliability.

In summary, our proposed framework, namely SIR-INN, provides an efficient and accurate surrogate for learning epidemiological models, enabling less costly forecasting while maintaining both generalizability and accuracy, even in long-term predictions. Given its simple design and interpretability, the model offers valuable insight into more efficient implementations of hybrid models for forecasting other dynamical systems with uncertainty quantification. A natural and immediate extension of this work is its application to other SIR-based epidemic models. In fact, it would only require retraining the neural network once after selecting parameter ranges that are better aligned with the specific disease under study. Furthermore, an interesting direction for generalization is the prediction of epidemics coupled with human behavior changes. In such cases, the individual approaches—the mechanistic modeling and the neural network component—remain limited by their partial perspectives on the system, failing to benefit from one another during the forecasting process. In conclusion, our work represents an initial step toward an increased integration of AI tools with mechanistic epidemic models to improve forecasting approaches, and contributes to the establishment of new standards in hybrid modeling.

## Code Availability

The code is available upon publication.

## CRediT authorship contribution statement

**Martina Rama:** Conceptualization, Data curation, Formal analysis, Methodology, Software, Validation, Visualization, Writing – original draft, Writing – review and editing.  
**Gabriele Santin:** Conceptualization, Data curation, Formal analysis, Methodology, Software, Supervision, Validation, Visualization, Writing – review and editing. **Giulia Cencetti:** Conceptualization, Methodology, Supervision, Validation, Writing – review and editing.  
**Michele Tizzoni:** Conceptualization, Supervision, Validation, Writing – review and editing.  
**Bruno Lepri:** Conceptualization, Supervision, Validation, Writing – review and editing.

## Acknowledgements

Bruno Lepri acknowledge the support of the PNRR ICSC National Research Centre for High Performance Computing, Big Data and Quantum Computing (CN00000013), under the NRRP MUR program funded by the NextGenerationEU

## References

S. Berkhahn and M. Ehrhardt. A physics-informed neural network to model covid-19 infection and hospitalization scenarios. *Advances in continuous and discrete models*, 2022(1):61, 2022.

G. Bertaglia, C. Lu, L. Pareschi, and X. Zhu. Asymptotic-preserving neural networks for multiscale hyperbolic models of epidemic spread. *Mathematical Models and Methods in Applied Sciences*, 32(10):1949–1985, 2022.

M. Biggerstaff, S. Cauchemez, C. Reed, M. Gambhir, and L. Finelli. Estimates of the reproduction number for seasonal, pandemic, and zoonotic influenza: a systematic review of the literature. *BMC infectious diseases*, 14(1):1–20, 2014.

M. Biggerstaff, D. Alper, M. Dredze, S. Fox, I. C.-H. Fung, K. S. Hickmann, B. Lewis, R. Rosenfeld, J. Shaman, M.-H. Tsou, et al. Results from the centers for disease control and prevention’s predict the 2013–2014 influenza season challenge. *BMC infectious diseases*, 16:1–10, 2016.

N. I. Bosse, H. Gruson, A. Cori, E. van Leeuwen, S. Funk, and S. Abbott. Evaluating forecasts with scoringutils in r. *arXiv preprint arXiv:2205.07090*, 2022.

J. Bracher, E. L. Ray, T. Gneiting, and N. G. Reich. Evaluating epidemic forecasts in an interval format. *PLoS computational biology*, 17(2):e1008618, 2021.

J. S. Brownstein, S. Chu, A. Marathe, M. V. Marathe, A. T. Nguyen, D. Paolotti, N. Perra, D. Perrotta, M. Santillana, S. Swarup, et al. Combining participatory influenza surveillance with modeling and forecasting: Three alternative approaches. *JMIR public health and surveillance*, 3(4):e7344, 2017.

S. Cai, Z. Mao, Z. Wang, M. Yin, and G. E. Karniadakis. Physics-informed neural networks (pinns) for fluid mechanics: A review. *Acta Mechanica Sinica*, 37(12):1727–1738, 2021.

F. Carrat, E. Vergu, N. M. Ferguson, M. Lemaitre, S. Cauchemez, S. Leach, and A.-J. Valleron. Time lines of infection and disease in human influenza: a review of volunteer challenge studies. *American journal of epidemiology*, 167(7):775–785, 2008.

S. Cuomo, V. S. Di Cola, F. Giampaolo, G. Rozza, M. Raissi, and F. Piccialli. Scientific machine learning through physics-informed neural networks: Where we are and what's next. *Journal of Scientific Computing*, 92(3):88, 2022.

S. Y. Del Valle, B. H. McMahon, J. Asher, R. Hatchett, J. C. Lega, H. E. Brown, M. E. Leany, Y. Pantazis, D. J. Roberts, S. Moore, et al. Summary results of the 2014-2015 darpa chikungunya challenge. *BMC infectious diseases*, 18:1–14, 2018.

A. N. Desai, M. U. Kraemer, S. Bhatia, A. Cori, P. Nouvellet, M. Herringer, E. L. Cohn, M. Carrión, J. S. Brownstein, L. C. Madoff, et al. Real-time epidemic forecasting: challenges and opportunities. *Health security*, 17(4):268–275, 2019.

L. C. Evans. *Partial differential equations*, volume 19. American Mathematical Society, 2022.

S. Fiandrino, A. Bizzotto, G. Guzzetta, S. Merler, F. Baldo, E. Valdano, A. M. Urdiales, A. Bella, F. Celino, L. Zino, et al. Collaborative forecasting of influenza-like illness in italy: the influcast experience. *Epidemics*, page 100819, 2025.

G. B. Folland. *Introduction to partial differential equations*, volume 102. Princeton university press, 1995.

S. J. Fox, M. Kim, L. A. Meyers, N. G. Reich, and E. L. Ray. Optimizing disease outbreak forecast ensembles. *Emerging Infectious Diseases*, 30(9):1967, 2024.

S. Funk, A. Camacho, A. J. Kucharski, R. Lowe, R. M. Eggo, and W. J. Edmunds. Assessing the performance of real-time epidemic forecasts: A case study of ebola in the western area region of sierra leone, 2014-15. *PLoS computational biology*, 15(2):e1006785, 2019.

I. Goodfellow, Y. Bengio, and A. Courville. *Deep learning*. MIT press, 2016.

J. M. Heffernan, R. J. Smith, and L. M. Wahl. Perspectives on the basic reproductive ratio. *Journal of the Royal Society Interface*, 2(4):281–293, 2005.

K. M. Holcomb, S. Mathis, J. E. Staples, M. Fischer, C. M. Barker, C. B. Beard, R. J. Nett, A. C. Keyel, M. Marcantonio, M. L. Childs, et al. Evaluation of an open forecasting challenge to assess skill of west nile virus neuroinvasive disease prediction. *Parasites & Vectors*, 16(1):11, 2023.

InfluCast. InfluCast - web platform, 2025. URL <https://influcast.org/>. Accessed: 26 April 2025.

Istituto Superiore di Sanità. Sistema di sorveglianza integrata respivirnet, istituto superiore di sanità. <https://www.epicentro.iss.it/influenza/respivirnet>, 2020. Accessed: 26 April 2025.

M. A. Johansson, K. M. Apfeldorf, S. Dobson, J. Devita, A. L. Buczak, B. Baugher, L. J. Moniz, T. Bagley, S. M. Babin, E. Guven, et al. An open challenge to advance probabilistic forecasting for dengue epidemics. *Proceedings of the National Academy of Sciences*, 116(48):24268–24274, 2019.

G. E. Karniadakis, I. G. Kevrekidis, L. Lu, P. Perdikaris, S. Wang, and L. Yang. Physics-informed machine learning. *Nature Reviews Physics*, 3(6):422–440, 2021.

W. O. Kermack and A. G. McKendrick. A contribution to the mathematical theory of epidemics. *Proceedings of the royal society of london. Series A, Containing papers of a mathematical and physical character*, 115(772):700–721, 1927.

E. Kharazmi, M. Cai, X. Zheng, Z. Zhang, G. Lin, and G. E. Karniadakis. Identifiability and predictability of integer-and fractional-order epidemiological models using physics-informed neural networks. *Nature Computational Science*, 1(11):744–753, 2021.

J. H. Lagergren, J. T. Nardini, R. E. Baker, M. J. Simpson, and K. B. Flores. Biologically-informed neural networks guide mechanistic modeling from sparse experimental data. *PLoS computational biology*, 16(12):e1008462, 2020.

S. A. Lauer, A. C. Brown, and N. G. Reich. Infectious disease forecasting for public health. In J. M. Drake, M. B. Bonsall, and M. R. Strand, editors, *Population biology of vector-borne diseases*, chapter 4, pages 45–68. Oxford University Press, Publisher’s location, edition (if applicable) edition, 2021.

Y. LeCun, Y. Bengio, and G. Hinton. Deep learning. *nature*, 521(7553):436–444, 2015.

K. Linka, A. Schäfer, X. Meng, Z. Zou, G. E. Karniadakis, and E. Kuhl. Bayesian physics informed neural networks for real-world nonlinear dynamical systems. *Computer Methods in Applied Mechanics and Engineering*, 402:115346, 2022.

V. K. Lopez, E. Y. Cramer, R. Pagano, J. M. Drake, E. B. O’Dea, M. Ade, T. Ayer, J. Chhatwal, O. O. Dalgic, M. A. Ladd, et al. Challenges of covid-19 case forecasting in the us, 2020–2021. *PLoS computational biology*, 20(5):e1011200, 2024.

W. G. Madden, W. Jin, B. Lopman, A. Zufle, B. Dalziel, C. J. E. Metcalf, B. T. Grenfell, and M. S. Lau. Deep neural networks for endemic measles dynamics: Comparative analysis and integration with mechanistic models. *PLOS Computational Biology*, 20(11):e1012616, 2024.

Z. Mao, A. D. Jagtap, and G. E. Karniadakis. Physics-informed neural networks for high-speed flows. *Computer Methods in Applied Mechanics and Engineering*, 360:112789, 2020.

P. R. Miles. pymcmcstat: A python package for bayesian inference using delayed rejection adaptive metropolis. *Journal of Open Source Software*, 4(38):1417, 2019. doi: 10.21105/joss.01417. URL <https://doi.org/10.21105/joss.01417>.

C. Millevoi, D. Pasetto, and M. Ferronato. A physics-informed neural network approach for compartmental epidemiological models. *PLOS Computational Biology*, 20(9):e1012387, 2024.

R. M. Neal. Probabilistic inference using markov chain monte carlo methods. 1993.

X. Ning, J. Guan, X.-A. Li, Y. Wei, and F. Chen. Physics-informed neural networks integrating compartmental model for analyzing covid-19 transmission dynamics. *Viruses*, 15(8):1749, 2023a.

X. Ning, L. Jia, Y. Wei, X.-A. Li, and F. Chen. Epi-dnns: Epidemiological priors informed deep neural networks for modeling covid-19 dynamics. *Computers in biology and medicine*, 158:106693, 2023b.

K. Nixon, S. Jindal, F. Parker, N. G. Reich, K. Ghobadi, E. C. Lee, S. Truelove, and L. Gardner. An evaluation of prospective covid-19 modelling studies in the usa: from data to science translation. *The Lancet Digital Health*, 4(10):e738–e747, 2022.

E. B. O’Dea and J. M. Drake. A semi-parametric, state-space compartmental model with time-dependent parameters for forecasting covid-19 cases, hospitalizations and deaths. *Journal of the Royal Society Interface*, 19(187):20210702, 2022.

A. Paszke, S. Gross, F. Massa, A. Lerer, J. Bradbury, G. Chanan, T. Killeen, Z. Lin, N. Gimelshein, L. Antiga, A. Desmaison, A. Kopf, E. Yang, Z. DeVito, M. Raison, A. Tejani, S. Chilamkurthy, B. Steiner, L. Fang, J. Bai, and S. Chintala. Pytorch: An imperative style, high-performance deep learning library. In *Advances in Neural Information Processing Systems 32*, pages 8024–8035. Curran Associates, Inc., 2019. URL <http://papers.neurips.cc/paper/9015-pytorch-an-imperative-style-high-performance-deep-learning-library.pdf>.

D. Perrotta, M. Tizzoni, and D. Paolotti. Using participatory web-based surveillance data to improve seasonal influenza forecasting in italy. In *Proceedings of the 26th International Conference on World Wide Web*, pages 303–310, 2017.

M. Raissi, P. Perdikaris, and G. E. Karniadakis. Physics-informed neural networks: A deep learning framework for solving forward and inverse problems involving nonlinear partial differential equations. *Journal of Computational physics*, 378:686–707, 2019.

E. L. Ray, Y. Wang, R. D. Wolfinger, and N. G. Reich. Flusion: Integrating multiple data sources for accurate influenza predictions. *Epidemics*, 50:100810, 2025.

N. G. Reich, C. J. McGowan, T. K. Yamana, A. Tushar, E. L. Ray, D. Osthus, S. Kandula, L. C. Brooks, W. Crawford-Crudell, G. C. Gibson, et al. Accuracy of real-time multi-model ensemble forecasts for seasonal influenza in the us. *PLoS computational biology*, 15(11):e1007486, 2019.

RespiVirNet, 2020. Respivirnet data extracts, 2020. URL <https://github.com/fbranda/influnet>. Accessed: 26 April 2025.

M. Richey. The evolution of markov chain monte carlo methods. *The American Mathematical Monthly*, 117(5):383–413, 2010.

A. Rodríguez, J. Cui, N. Ramakrishnan, B. Adhikari, and B. A. Prakash. Einns: epidemiologically-informed neural networks. In *Proceedings of the AAAI Conference on Artificial Intelligence*, volume 37, pages 14453–14460, 2023.

A. Rodríguez, H. Kamarthi, P. Agarwal, J. Ho, M. Patel, S. Sapre, and B. A. Prakash. Machine learning for data-centric epidemic forecasting. *Nature Machine Intelligence*, 6(10):1122–1131, 2024.

S. Shaier, M. Raissi, and P. Seshaiyer. Data-driven approaches for predicting spread of infectious diseases through dinns: Disease informed neural networks. *arXiv preprint arXiv:2110.05445*, 2021.

K. Sherratt, H. Gruson, H. Johnson, R. Niehus, B. Prasse, F. Sandmann, J. Deuschel, D. Wolffram, S. Abbott, A. Ullrich, et al. Predictive performance of multi-model ensemble forecasts of covid-19 across european nations. *Elife*, 12:e81916, 2023.

Y. Shi, P. Wei, K. Feng, D.-C. Feng, and M. Beer. A survey on machine learning approaches for uncertainty quantification of engineering systems. *Machine Learning for Computational Science and Engineering*, 1(1):1–39, 2025.

C. Viboud, K. Sun, R. Gaffey, M. Ajelli, L. Fumanelli, S. Merler, Q. Zhang, G. Chowell, L. Simonsen, A. Vespignani, et al. The rapidd ebola forecasting challenge: Synthesis and lessons learnt. *Epidemics*, 22:13–21, 2018.

M. L. Waskom. seaborn: statistical data visualization. *Journal of Open Source Software*, 6(60):3021, 2021. doi: 10.21105/joss.03021. URL <https://doi.org/10.21105/joss.03021>.

D. Wolffram, S. Abbott, M. An der Heiden, S. Funk, F. Günther, D. Hailer, S. Heyder, T. Hotz, J. van de Kassteele, H. Küchenhoff, et al. Collaborative nowcasting of covid-19 hospitalization incidences in germany. *PLOS Computational Biology*, 19(8):e1011394, 2023.

Y. Ye, A. Pandey, C. Bawden, D. M. Sumsuzzman, R. Rajput, A. Shoukat, B. H. Singer, S. M. Moghadas, and A. P. Galvani. Integrating artificial intelligence with mechanistic epidemiological modeling: a scoping review of opportunities and challenges. *Nature Communications*, 16(1):1–18, 2025.

Q. Zhang, C. Gioannini, D. Paolotti, N. Perra, D. Perrotta, M. Quaggiotto, M. Tizzoni, and A. Vespignani. Social data mining and seasonal influenza forecasts: the fluoutlook platform. In *Machine Learning and Knowledge Discovery in Databases: European Conference, ECML PKDD 2015, Porto, Portugal, September 7-11, 2015, Proceedings, Part III 15*, pages 237–240. Springer, 2015.

## 6 Additional plots

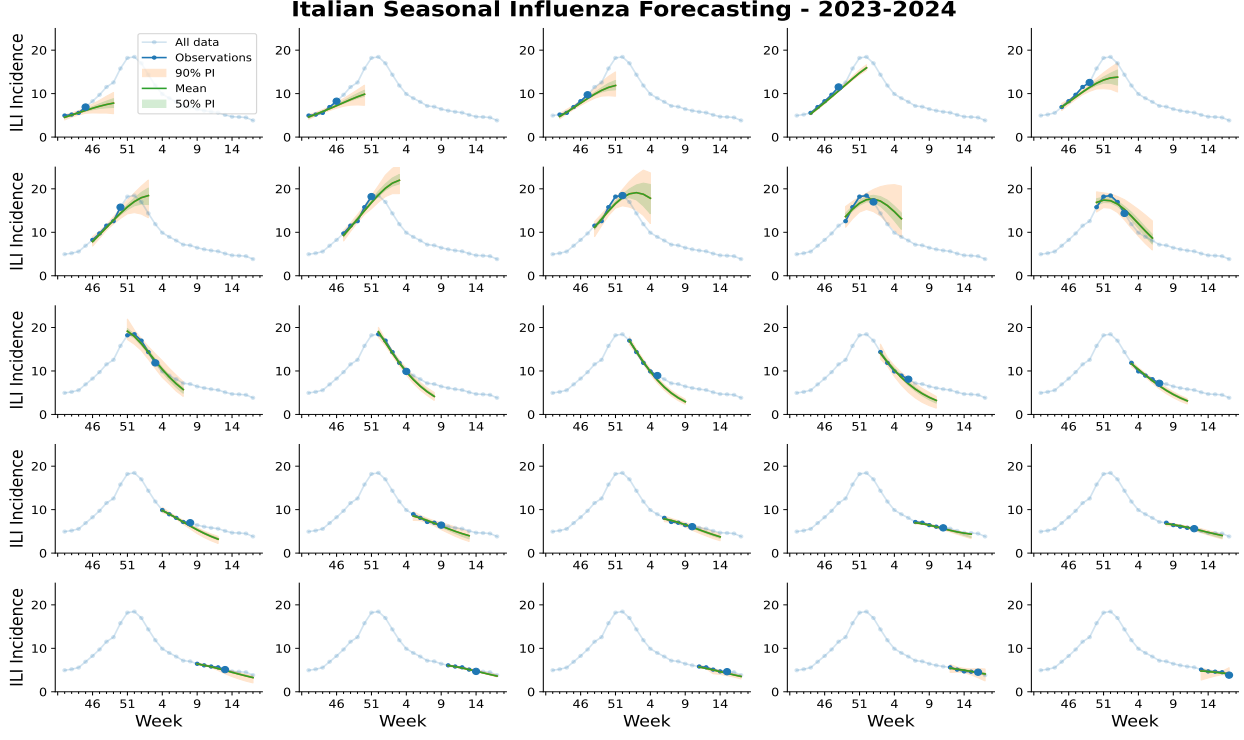


Figure 6: **Seasonal influenza forecasting four weeks ahead via SIR-INN.** The ground truth data, in blue, represent the weekly observations at national level of the 2023-2024 seasonal influenza. The highlighted blue data represent the time window of observations, with fixed length of 5, from which the SIR-based PINN infers the epidemic parameters and then forecasts on the following four weeks ahead. The mean-model fits and forecasts are represented with green lines and the 50% and 90% percentile intervals are shaded, respectively, in green and orange error bars.

### Italian Seasonal Influenza Forecasting - 2024-2025

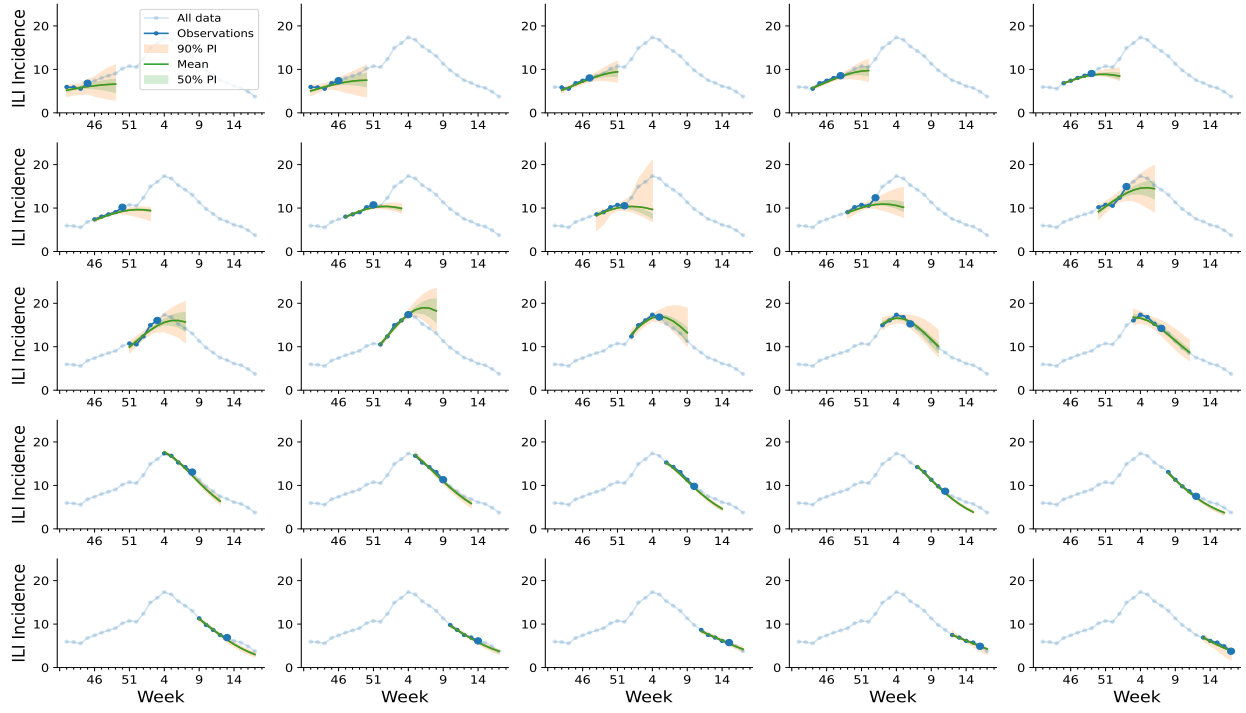


Figure 7: **Seasonal influenza forecasting four weeks ahead via SIR-INN.** The ground truth data, in blue, represent the weekly observations at national level of the 2024-2025 seasonal influenza. The highlighted blue data represent the time window of observations, with fixed length of 5, from which the SIR-based PINN infers the epidemic parameters and then forecasts on the following four weeks ahead. The mean-model fits and forecasts are represented with green lines and the 50% and 90% percentile intervals are shaded, respectively, in green and orange error bars.

## Italian Seasonal Influenza Long-Term Forecasting - 2024-2025

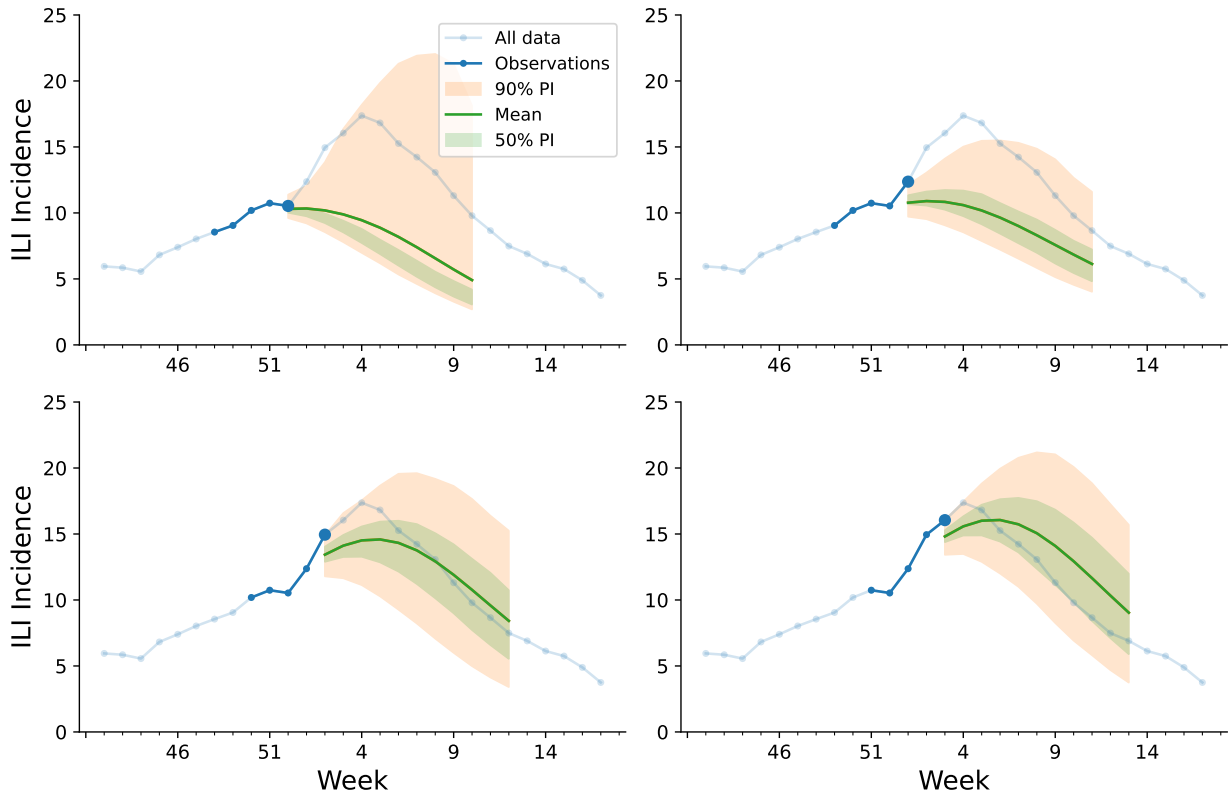


Figure 8: **Seasonal influenza forecasting ten weeks ahead via SIR-INN.** The ground truth data, in blue, represent the weekly observations at national level of the 2024-2025 seasonal influenza. The highlighted blue data represent the time window of observations, with fixed length of 5, from which the SIR-based PINN infers the epidemic parameters and then forecasts on the following ten weeks ahead. The mean-model forecasts are represented with green lines and the 50% and 90% percentile intervals are shaded, respectively, in green and orange error bars.